Microbial Pathogenesis 217 (2026) 108580

Contents lists available at ScienceDirect

Microbial Pathogenesis

journal homepage: www.elsevier.com/locate/micpath

Silver nanoparticles biosynthesized by *Citrobacter farmeri* effectively inhibit growth and biofilm formation in *Acinetobacter baumannii*

Sazan Moffaq Abdulaziz [a], Sayran H. Haji [b], Aryan R. Ganjo [b,c], Safaa Toma Hanna Aka [b], Nidhi Bhardwaj [d,e], Indu Bhardwaj [f], Soumya Ghosh [g,h,*]

[a] Department of Medical Laboratory Technology, Erbil Technical Health and Medical College, Erbil Polytechnic University, Erbil, Kurdistan-Region, Iraq
[b] Department of Clinical Analysis, College of Pharmacy, Hawler Medical University, Kurdistan Region, Iraq
[c] Department of Medical Analysis, Faculty of Applied Science, Tishk International University, Erbil, Iraq
[d] Center of Advanced Innovation Technologies, VŠB-Technical University of Ostrava, Poruba, Ostrava, 708 00, Czech Republic
[e] Department of Chemistry, Faculty of Science, University of Hradec Kralove, Rokitanskeho 62, Hradec Kralove, 500 03, Czech Republic
[f] Division of Microbiology, Career Point University, Hamirpur, Himachal Pradesh, 176041, India
[g] Natural and Medical Sciences Research Center, University of Nizwa, Nizwa, 616, Oman
[h] University of the Free State, Bloemfontein, 9301, South Africa

ARTICLE INFO

Keywords:
Acinetobacter baumannii
AgNPs
Antibacterial activity
Anti-Biofilm activity
Carbapenem resistance
Multi-drug resistant

ABSTRACT

The emergence of carbapenem-resistant *Acinetobacter baumannii* (*A. baumannii*) has severely limited available therapeutic options, posing a significant clinical challenge. This study aimed to evaluate the antibacterial and antibiofilm efficacy of biosynthesized silver nanoparticles (AgNPs) against clinical multi-drug resistant (MDR) *A. baumannii* isolates. Silver nanoparticles were biosynthesized using *Citrobacter farmeri* (*C. farmeri*) (A121) and subsequently characterized for their physicochemical properties. Antibacterial activity against *A. baumannii* was assessed using the disc diffusion assay, while biofilm-forming ability and antibiofilm efficacy were evaluated using the microtiter plate method. Molecular analysis revealed a high prevalence of resistance-associated genes, with $bla_{\text{OXA-48}}$ (70%), $bla_{\text{CTX-M}}$ (43%), and bla_{DHA} (13.3%) being the most frequently detected ESBL-, AmpC-, and carbapenemase-encoding genes, respectively. Notably, 65.3% of the isolates exhibited strong biofilm-forming capacity. The biosynthesized AgNPs ranged in size from 20 to 60 nm and demonstrated a pronounced, concentration-dependent antibacterial effect at 1.25, 2.5, and 5 mg/mL. Moreover, AgNP treatment resulted in a substantial inhibition of biofilm formation, achieving up to 95% reduction (2.5 mg/mL). Overall, these findings highlight the potent antibacterial and antibiofilm activities of biosynthesized AgNPs against MDR *A. baumannii*, highlighting their potential as a promising alternative or adjunctive strategy for combating infections caused by highly drug-resistant pathogens.

1. Introduction

A. baumannii is widely recognized as one of the most challenging MDR bacterial pathogens, owing to its notable ability to rapidly acquire and express a broad spectrum of antimicrobial resistance determinants that severely compromise therapeutic efficacy [1]. Its persistence and success in hospital environments are largely attributed to its strong capacity to adhere to both biotic and abiotic surfaces and to form biofilms on medical devices and hospital infrastructure [2]. Biofilm-associated cells exhibit intrinsic tolerance to antimicrobial agents, primarily due to impaired drug penetration, reduced metabolic activity, and the presence of dormant or slowly proliferating bacterial populations [3]. Consequently, *A. baumannii* biofilms display markedly reduced susceptibility to multiple classes of antibiotics, facilitating chronic infections and treatment failure [4].

Carbapenems have traditionally been regarded as last-resort antibiotics for managing severe infections caused by MDR Gram-negative bacteria, due to their broad-spectrum activity, stability against most β-lactamases, strong affinity for penicillin-binding proteins, and favorable safety profiles [5]. However, the global emergence and dissemination of carbapenem-resistant *A. baumannii* have significantly narrowed available treatment options and represents a major clinical concern [6]. Carbapenem resistance may arise through the production of carbapenemases or via alternative mechanisms, including reduced outer

* Corresponding author. Natural and Medical Sciences Research Center, University of Nizwa, Nizwa, 616, Oman.
E-mail addresses: soumyaghosh@yahoo.com, s.ghosh@unizwa.edu.om (S. Ghosh).

https://doi.org/10.1016/j.micpath.2026.108580
Received 7 March 2026; Received in revised form 23 April 2026; Accepted 20 May 2026
Available online 21 May 2026
0882-4010/© 2026 Elsevier Ltd. All rights are reserved, including those for text and data mining, AI training, and similar technologies.

membrane permeability, overexpression of efflux pumps, and the combined activity of extended-spectrum β-lactamases (ESBLs) or AmpC β-lactamases [7]. Accurate laboratory detection of carbapenemase production is therefore essential for guiding appropriate antimicrobial therapy, updating treatment guidelines, and elucidating molecular mechanisms underlying therapeutic failure [8]. The increasing prevalence of carbapenem-resistant *A. baumannii* has been associated with prolonged hospital stays, elevated healthcare costs, and increased mortality rates [5].

Given these challenges, the development of alternative or adjunctive antimicrobial strategies is urgently needed. On the other hand, nanotechnology has emerged as a promising approach for enhancing the antimicrobial properties of metals through their conversion into nanoparticles (NPs), which often exhibit synergistic effects when combined with conventional antibiotics [9,10]. Nanoparticles are generally more stable and may exhibit lower toxicity compared to traditional antimicrobial agents [11]. Among inorganic nanomaterials, silver nanoparticles (AgNPs) have attracted considerable attention due to their potent and broad-spectrum antimicrobial activity [12,13]. AgNPs exert their effects through multiple mechanisms, including disruption of bacterial membranes, interference with ion transport, enzyme inhibition, modulation of gene expression, and induction of oxidative stress–mediated cell death pathways.

Previous studies have demonstrated the efficacy of biosynthesized AgNPs against a wide range of pathogenic bacteria. For instance, Siddiqui et al. [14] reported that AgNPs synthesized using *Lactobacillus casei* exhibited strong antibacterial and antibiofilm activity, significantly reducing quorum-sensing-regulated virulence factor production. Similarly, Sheng et al. [15] demonstrated that *Ruellia tuberosa*-derived AgNPs effectively inhibited several clinically important pathogens, with enhanced antibacterial activity observed when combined with conventional antibiotics and minimal hemolytic toxicity. These findings highlight the potential of AgNP-based combination therapies as a viable strategy to overcome antimicrobial resistance [16].

The current understanding of biosynthesized AgNPs extends far beyond isolated examples from single Gram-positive bacteria or plant species, representing a robust and diverse field with demonstrated efficacy across multiple biological kingdoms. Recent studies have successfully employed a wide spectrum of microbial and botanical sources for AgNP biosynthesis, including Gram-negative bacteria such as *Citrobacter* spp., *Pseudomonas* spp., and *Escherichia coli* [17],

Gram-positive bacteria like *Bacillus* spp [18]. and *Lactobacillus* spp. [19], diverse fungal species [20], and numerous plant extracts including lemongrass (*Cymbopogon citratus*) and *Adenanthera pavonina* [21]. These biosynthesized AgNPs consistently demonstrate potent, concentration-dependent antibacterial activity against both Gram-positive (e.g., *Staphylococcus aureus*, *Enterococcus faecalis*) and Gram-negative (e.g., *Escherichia coli*, *Pseudomonas aeruginosa*, *Klebsiella pneumoniae*) pathogens [22], with particular effectiveness often observed against multidrug-resistant clinical isolates [17]. The enhanced antibacterial properties are attributed not only to the intrinsic biocidal effects of silver ions but also to the synergistic contributions of biomolecular capping agents derived from the synthesis organisms, which improve nanoparticle stability, cellular uptake, and target specificity [23]. This extensive body of evidence underscores biosynthesized AgNPs as a versatile and well-validated platform for developing next-generation antimicrobial agents, rather than an approach limited to a narrow range of biological sources.

In this context, the present study aims to investigate the prevalence of multidrug resistance in clinical isolates of *A. baumannii* and to evaluate the antibacterial and antibiofilm activities of biosynthesized AgNPs produced using *Citrobacter farmeri*. Furthermore, the study assesses the impact of AgNPs on biofilm formation in MDR *A. baumannii* isolates obtained from clinical settings in Erbil, Kurdistan Region of Iraq.

2. Materials and methods

2.1. Collection of clinical samples

A total of 91 non-duplicate clinical isolates of *Acinetobacter baumannii* were recovered from diverse infection sites, including urine (n = 24), sputum (n = 16), wound swabs (n = 8), and blood (n = 3). Clinical specimens were obtained between January and December 2022 from both hospitalized and community-acquired infections at Rizgary Teaching Hospital, Erbil, Kurdistan Region of Iraq. The median age of the patients was 40 years (range: 0-80 years), with females accounting for 60.3% (n = 47) of the study population.

2.2. Clinical bacterial isolation, identification and selection

The collected clinical specimens were initially processed for bacterial isolation. Samples were cultured on Trypticase Soy Agar (TSA), and pure isolates were obtained through repeated subculturing using the streak plate technique. Preliminary identification was based on morphological and biochemical characteristics, followed by confirmation using the automated Vitek-2 system (bioMérieux, USA) with Gram-negative (GN) identification cards, in accordance with the manufacturer's instructions. Confirmed isolates were preserved as single colonies in Trypticase Soy Broth (TSB) containing 20% glycerol and stored at −70 °C until further analysis [24].

Furthermore, molecular identification of the bacterial isolates was performed following a previously described protocol [25] using the primers PA-SS-F (5′-CAGCTCGTGTCGTGAGATGT-3′) and PA-SS-R (5′-CGTAAGGGCCATGACTT-3′) as described earlier [26].

PCR amplicons were sequenced at the National Instrumentation Centre for Environmental Management, Seoul, Korea. The obtained nucleotide sequences were analyzed using the BLAST algorithm against sequences available in the GenBank database (NCBI) [27]. Isolates exhibiting greater than 98% sequence similarity to reference entries were considered correctly identified, and the validated sequences were subsequently submitted to GenBank to obtain accession numbers.

In addition, phylogenetic analysis of the *C. farmeri* isolates was conducted using MEGA version 11 [28]. Partial 16S rRNA gene sequences were aligned with closely related reference sequences retrieved from the NCBI GenBank database. Phylogenetic reconstruction was performed using the Neighbor-Joining (NJ) method [29], and the robustness of the inferred tree topology was evaluated by bootstrap analysis [30]. Evolutionary distances were calculated using the p-distance model [31], expressed as the number of base substitutions per site. The resulting phylogenetic tree was drawn to scale, with branch lengths corresponding to the computed evolutionary distances. The analysis included a total of 11 nucleotide sequences. All positions containing gaps and missing data were excluded using the complete deletion option, yielding a final dataset of 104 aligned positions. The representative sequence generated in this study was deposited in the NCBI GenBank database, and an accession number was assigned accordingly.

Based on the comprehensive identification results, five *C. farmeri* isolates were selected for the biosynthesis of silver nanoparticles (AgNPs). Additionally, a total of 91 non-duplicate clinical isolates of *A. baumannii* exhibiting MDR, including carbapenem resistance, were included to evaluate the antibacterial efficacy of the biosynthesized AgNPs.

2.3. Biosynthesis and characterization of AgNPs

The biosynthesis of AgNPs was performed following a previously described protocol [32]. Five *C. farmeri* strains (A120, A121, A122, A123, and A124) were screened for their ability to synthesize AgNPs, of which only strain A121 exhibited positive nanoparticle formation. Briefly, the selected *C. farmeri* strain was cultured in 100 mL of sterile trypticase soy broth (TSB; Oxoid) and incubated at 35 °C with shaking at

120 rpm for 24 h. The culture was then centrifuged at 10,000 rpm for 10 min, and the cell-free supernatant was collected. The supernatant was mixed with 10 mM silver nitrate ($AgNO_3$; Sigma-Aldrich, USA; 99.9% purity) in a 1:1 (v/v) ratio and incubated in the dark at 35 °C for 24 h. A control consisting of TSB mixed with culture supernatant without $AgNO_3$ was maintained under identical conditions. The formation of AgNPs was initially indicated by a visible color change from pale yellow to dark brown. The nanoparticles were recovered by centrifugation at 8000 rpm for 15 min at 4 °C, followed by repeated washing with distilled water. The resulting pellet was dried overnight in a hot-air oven at 60 °C. The dried dark-brown material was scraped, powdered, and stored in an airtight glass container for further characterization [33].

The synthesized AgNPs were characterized using a UV-visible spectrophotometer (PerkinElmer Lambda 35, USA) to record the surface plasmon resonance peak over a wavelength range of 300–800 nm, with double-distilled water used as the reference blank [34]. Fourier-transform infrared (FT-IR) spectroscopy (JASCO Spectrum 4600) was employed to identify the functional groups associated with AgNP formation. Spectral analysis was performed in the range of 4000-400 cm^{-1} at a resolution of 4 cm^{-1} [32].

The crystalline nature and phase composition of the AgNPs were determined by X-ray diffraction (XRD) analysis using a PANalytical X'Pert PRO diffractometer with Cu Kα radiation (λ = 1.5406 Å), operated at 40 kV and 40 mA. Diffraction patterns were recorded over a 2θ range of 20°–80°, using dried AgNP powder samples mounted on the XRD sample holder [33].

The morphology and particle size distribution of the AgNPs were examined using advanced transmission electron microscopy (TEM; Titan^3 G2 60–300, FEI, USA) and field-emission scanning electron microscopy (FE-SEM; Quanta 4500). For TEM analysis, AgNPs were deposited as a thin film onto copper grids coated with holey carbon and air-dried prior to imaging [35]. The elemental composition of the AgNPs was further analyzed using energy-dispersive X-ray spectroscopy (EDX) coupled with FE-SEM, with samples prepared on carbon-coated copper grids [36,37].

2.4. Antibacterial susceptibility to conventional antibiotics

The antimicrobial agents evaluated included piperacillin and piperacillin-tazobactam (penicillins); ceftazidime (cephalosporin); tobramycin, netilmicin, and gentamicin (aminoglycosides); ciprofloxacin and levofloxacin (fluoroquinolones); imipenem and meropenem (carbapenems); trimethoprim/sulfamethoxazole (sulfonamides); and tigecycline (tetracycline). Antimicrobial susceptibility testing of *A. baumannii* isolates was performed using the Vitek® 2 automated system, following the manufacturer's instructions. Resistance profiles were categorized as MDR according to the criteria described in a previous study [38]. *Pseudomonas aeruginosa* ATCC 27853 was used as the quality control strain to validate the accuracy and reliability of the susceptibility testing procedures.

2.5. PCR screening for β-lactamase genes

Polymerase chain reaction (PCR) screening was performed on 30 *A. baumannii* isolates to detect genes encoding extended-spectrum β-lactamases (ESBLs) (*bla* $_{CTX}$, *bla* $_{TEM}$, *bla* $_{SHV}$), AmpC β-lactamases (*bla* $_{CY1}$, *bla* $_{CY2}$, *bla* $_{DHA}$, *bla* $_{FOX}$), and carbapenemases (*bla* $_{IMP}$, *bla* $_{NDM}$, *bla* $_{VIM}$, *bla* $_{KPC}$, *bla* $_{OXA-48}$). The selection was based on stratified random sampling to ensure representation across key phenotypic and epidemiological variables observed among the full cohort of 91 *Acinetobacter baumannii* isolates. Specifically, isolates were first grouped by: (i) biofilm-forming capacity (strong, moderate, weak, non-producer), (ii) resistance profile heterogeneity (e.g., presence/absence of tigecycline resistance, which showed variability unlike the uniformly MDR background), and (iii) source of specimens (blood, urine, pus, etc …). Within each stratum, isolates were randomly selected to achieve proportional representation — resulting in 30 strains covering all four biofilm categories and both specimens' types, with balanced distribution across resistance sub patterns. Moreover, gene-specific primers previously described by Poirel et al. [39] were employed for amplification.

Genomic DNA was extracted from bacterial cultures in the logarithmic growth phase using a commercial DNA extraction kit (DNAL and Scientific, Cat. No. GG2001; Viogene Biotech Corp., New Taipei City, Taiwan), according to the manufacturer's instructions. PCR amplification was carried out in a final reaction volume of 25 μL contained 1 μL of each primer (10 μM), 12.5 μL of 2× Taq Green PCR Master Mix (Thermo Fisher Scientific Inc., USA), 1 μL of template DNA, and 9.5 μL of nuclease-free water.

The PCR cycling conditions comprised an initial denaturation step at 94 °C for 10 min, followed by 35 cycles of denaturation at 94 °C for 30 s, annealing at 54 °C for 30 s, and extension at 72 °C for 1 min, with a final extension at 72 °C for 7 min. Amplified PCR products were resolved by electrophoresis on 2% (w/v) agarose gels and visualized under UV illumination.

2.6. Biofilm formation assay

Biofilm formation was assessed using the microtiter plate assay, as previously described [40]. Briefly, all isolates of *A. baumannii* were cultured overnight in 5 mL of trypticase soy broth (TSB; Merck, Germany) at 37 °C. The overnight cultures were then diluted 1:100 in fresh TSB, and 200 μL of the diluted suspension was dispensed into individual wells of sterile 96-well polystyrene microtiter plates (Costar, USA). Plates were incubated at 37 °C for 24 h under static conditions.

Following incubation, the culture medium was gently aspirated, and the wells were washed three times with 200 μL of phosphate-buffered saline (PBS; pH 7.2) to remove non-adherent cells. The plates were air-dried and subsequently stained with 200 μL of 0.1% (w/v) crystal violet for 30 min at room temperature. Excess stain was removed by rinsing the wells with distilled water, and the plates were allowed to dry completely. The bound crystal violet was solubilized by adding 200 μL of 95% ethanol to each well.

The optical density (OD) of the solubilized dye was measured at 630 nm using an ELISA plate reader [40]. Biofilm formation was categorized based on OD values as follows: non-biofilm producers (OD < 0.12), weak biofilm producers (OD = 0.12-0.24), and strong biofilm producers (OD > 0.24). All experiments were performed in triplicate on three independent occasions, and results were expressed as mean OD values [41].

2.7. Antimicrobial activity of biosynthesized AgNPs

The antibacterial activity of the biosynthesized AgNPs was evaluated using the disc diffusion method against multidrug-resistant *A. baumannii*, as previously described [42]. Briefly, bacterial suspensions of selected MDR *A. baumannii* isolates were adjusted to a turbidity equivalent to 1.5 × 10^8 CFU/mL and uniformly spread onto Mueller-Hinton agar (MHA) plates using sterile cotton swabs.

Sterile Whatman paper discs (6 mm diameter) were impregnated with 10 μL of AgNP suspensions at varying concentrations (5000, 2500, and 1250 μg/mL) and allowed to air-dry under aseptic conditions. Discs loaded with 10 μL of sterile distilled water served as negative controls. The prepared discs were aseptically placed onto the inoculated MHA plates, which were then incubated at 37 °C for 24 h.

Following incubation, the zones of inhibition (ZOI) surrounding the discs were measured and recorded in millimeters. All assays were performed in triplicate to ensure reproducibility, and the mean inhibition zone diameters were calculated.

2.8. Antibiofilm potential of AgNPs

The antibiofilm potential of the biosynthesized AgNPs was evaluated

using the 96-well microtiter plate assay, as previously described [43]. Briefly, each well of a sterile microtiter plate was loaded with 180 μL of Mueller-Hinton (MH) broth and inoculated with 10 μL of an overnight-grown bacterial culture. Subsequently, 10 μL of AgNP stock solution was added to each well to obtain final nanoparticle concentrations of 19.531, 39.0625, 78.125, 156.25, 312.5, 625, 1250, and 2500 μg/mL. Plates were incubated at 37 °C for 24 h under static conditions.

After incubation, the contents of the wells were carefully aspirated, and the wells were washed three times with 200 μL of phosphate-buffered saline (PBS; pH 7.2) to remove planktonic cells. The adherent biofilm formed by sessile cells was fixed with 2% (w/v) sodium acetate and stained with 0.1% (w/v) crystal violet. Excess stain was removed by rinsing the wells with sterile Milli-Q water, and the plates were allowed to air-dry. The bound crystal violet was then solubilized by adding 200 μL of 95% (v/v) ethanol to each well.

The absorbance was measured at 620 nm using an ELISA microplate reader (Multiskan® EX, Thermo Scientific, Finland), and the optical density values were used as an indicator of biofilm biomass. The percentage of biofilm inhibition was calculated using the formula:

% biofilm inhibition = [(1 − OD_{620} of AgNP-treated cells / OD_{620} of untreated control) × 100].

All experiments were performed in triplicate. A bacterial cell-free filtrate (10 μL) was used as the positive control during AgNP preparation.

2.9. Analysis of statistics

All data were analyzed using GraphPad Prism software. Statistical significance was assessed using the chi-square (χ^2) test, and a p value < 0.05 was considered statistically significant.

3. Results and discussion

3.1. Characteristics of bacterial isolates and demographic factors

In the present study, a total of 91 MDR *A. baumannii* isolates were recovered from a range of clinical specimens. Statistical analysis revealed a highly significant association between the type of clinical specimen and patient age group ($p < 0.001$), indicating that specimen distribution varied markedly across different age categories. Of the total isolates, 58 (63.7%) were obtained from male patients, while 33 (36.3%) were recovered from females, suggesting a higher susceptibility to infection among males.

This male predominance is consistent with previous reports from Iraq and Jordan, which documented a higher prevalence of *A. baumannii* infections among adult male patients, particularly those admitted to intensive care units with wound-related infections [44,45]. Similarly, Al-Tamimi et al. [46] reported a significantly higher incidence of MDR *A. baumannii* infections among male patients, especially within the 18-60 year age group, in Jordanian tertiary care hospitals, emphasizing the need for gender-specific surveillance and targeted infection control strategies.

Age-wise analysis demonstrated notable variability in infection rates, with the highest proportion of isolates recovered from patients aged 40–60 years (39.5%), followed by those aged 20–40 years (38.4%). In contrast, the lowest isolation rate was observed among patients aged between 1 month and 20 years. Furthermore, the majority of isolates were recovered from sputum samples (72.5%), followed by wound swabs (17.5%), blood samples (5.4%), and urine samples (4.3%) (Table 1).

The predominance of respiratory specimens highlights the significance of *A. baumannii* as a major pathogen associated with respiratory tract infections, particularly in hospitalized and critically ill patients.

Table 1
Demographic profile of patients and clinical specimen distribution of multidrug-resistant *A. baumannii* isolates (n = 91).

Variable	Category	No. of isolates	Percentage (%)
Sex	Male	58	63.7
	Female	33	36.2
Age	1 month-20 years	6	6.5
	20-40	35	38.4
	40-60	36	39.5
	60-80	15	16.4
Clinical specimen	Sputum	66	72.5
	Wound swab	16	17.5
	Blood	5	5.4
	Urine	4	4.3

Differences among demographic variables and specimen sources were statistically significant ($p < 0.001$).

These findings are in close agreement with previous studies, which reported sputum as the principal source of MDR *A. baumannii* isolates, followed by wound, urine, and blood samples [47,48]. Collectively, the observed distribution underscores the opportunistic nature of *A. baumannii* and its strong association with respiratory and wound infections in adult patient populations.

3.2. Antimicrobial resistance profile

Antimicrobial susceptibility testing performed using the Vitek® 2 automated system revealed that all 91 *A. baumannii* isolates exhibited high levels of resistance to the tested antimicrobial agents. Based on their frequent clinical use in hospital settings, 12 antibiotics representing seven major antimicrobial classes were selected for detailed antibiogram analysis. The resistance and susceptibility profiles of the isolates are summarized in Table 2.

A statistically significant variation in resistance rates was observed across different antimicrobial classes ($p < 0.001$). Notably, complete resistance (100%) was recorded against β-lactam antibiotics, including penicillins (piperacillin and piperacillin/tazobactam), cephalosporins (ceftazidime), and carbapenems (imipenem and meropenem), as well as against the aminoglycoside gentamicin. Among the antibiotics tested, tigecycline (tetracycline class) demonstrated the lowest resistance rate, with only 24 isolates (26.3%) showing resistance, indicating comparatively higher efficacy. Approximately, 75% of the MDR *A. baumannii* isolates remained susceptible to tigecycline, highlighting its potential as a therapeutic option against MDR infections.

The widespread escalation of antimicrobial resistance, particularly carbapenem resistance among Gram-negative bacilli, represents a major challenge to current treatment strategies and has been extensively

Table 2
Antimicrobial resistance profile of multidrug-resistant *A. baumannii* isolates (n = 91).

Antimicrobial classes	Antibiotics	Resistance isolates, n (%)
Carbapenem	Imipenem Meropenem	91 (100)
Cephalosporin	Ceftazidime	
Penicillins	Piperacillin Piperacillin/ tazobactam	
Sulfonamides	Trimethoprim-Sulfamethoxazole	78 (85.7)
Tetracycline	Tigecycline	24 (26.3)
Fluroquinolones	Levofloxacin	89 (97.8)
	Ciprofloxacin	87 (95.6)
Aminoglycoside	Gentamycin	91 (100)
	Tobramycin	77 (84.6)
	Netilmicin	79 (86.8)
Resistance phenotype	MDR	91 (100)

Overall resistance rates differed significantly across antimicrobial classes ($p < 0.001$).

reported worldwide. The clinical implications of carbapenem-resistant *A. baumannii* (CRAB) have reached the level of a global public health emergency [49]. In the present study, resistance to imipenem and meropenem was universal (100%), underscoring the critical severity of the resistance burden and corroborating recent public health alerts regarding the increasing prevalence of CRAB strains [40].

In addition to β-lactam resistance, high resistance rates were observed for fluoroquinolones, with 97.8% and 95.6% of isolates resistant to levofloxacin and ciprofloxacin, respectively. Overall, all isolates (100%) demonstrated resistance to at least three major antimicrobial classes, penicillins, cephalosporins, and carbapenems, thereby fulfilling the criteria for multidrug resistance. These findings emphasize the remarkable adaptability of *A. baumannii* and its capacity to survive under intense antimicrobial selective pressure.

The multidrug-resistant phenotype of *A. baumannii* can be attributed to multiple molecular mechanisms, including the acquisition of resistance genes via mobile genetic elements and chromosomal mutations affecting porins and efflux pumps, which collectively reduce intracellular antibiotic accumulation [44]. β-Lactam resistance, particularly to carbapenems, is frequently associated with alterations in penicillin-binding proteins (PBPs), which are essential for bacterial cell wall synthesis. Mutations or reduced expression of PBPs decrease the binding affinity of β-lactam antibiotics, thereby compromising their efficacy. Although eight PBPs have been identified in *A. baumannii*, only a limited number of mutations have been directly linked to antibiotic resistance, with many reported variations being phenotypically silent [50].

Furthermore, reduced permeability of the outer membrane plays a crucial role in carbapenem resistance. Transport of β-lactam antibiotics is mediated by porin channels and outer membrane proteins (OMPs), such as CarO, HMP-AB, and OmpW. Mutations or the loss of specific CarO isoforms (25- or 29-kDa) have been associated with carbapenem nonsusceptibility, rendering *A. baumannii* intrinsically resistant to this critical class of antibiotics [51].

Given the alarming resistance patterns observed, alternative therapeutic strategies are urgently required. Recent studies have highlighted the antibacterial potential of biologically synthesized nanoparticles. For example, gold nanoparticles (AuNPs) synthesized using *Proteus mirabilis* have demonstrated strong antibacterial activity against MDR Gram-negative pathogens, with minimum inhibitory concentrations ranging from 156 to 1250 μg/mL. Notably, these AuNPs exhibited synergistic effects when combined with conventional antibiotics, such as ceftriaxone, even at low concentrations, resulting in substantial enhancement of antibacterial efficacy [25]. Such nanotechnology-based approaches may represent promising adjunct or alternative therapies for combating MDR *A. baumannii* infections.

3.3. Biofilm production assay

Assessment of biofilm-forming ability among the 91 *A. baumannii* isolates revealed that 60 isolates (65.9%) were capable of producing biofilms. The distribution of biofilm-forming phenotypes is illustrated in Fig. 1. Using the tissue culture plate method, the majority of isolates demonstrated a strong biofilm-forming capacity (78.3%), while smaller proportions exhibited moderate (16.6%) and weak (5.0%) biofilm production. Statistical analysis showed no significant association between biofilm formation and the number of MDR *A. baumannii* isolates ($p > 0.05$).

The ability of *A. baumannii* to form biofilms is a critical virulence trait that facilitates prolonged environmental survival, host colonization, and persistence in hospital settings. Biofilm-embedded cells exhibit enhanced tolerance to antimicrobial agents, host immune defenses, and disinfectants, thereby complicating eradication once established [40]. This protective phenotype likely contributes to the high prevalence of chronic and recurrent infections associated with *A. baumannii*. Based on the experimental results, there is a significant correlation between

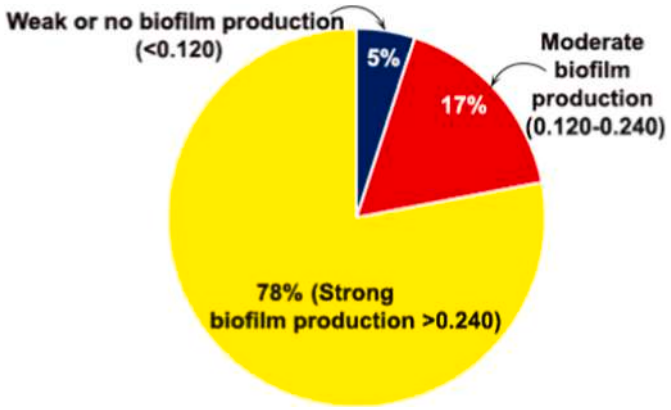

Fig. 1. Biofilm-producing capacities among 60 *A. baumannii* isolates. The pie chart shows the distribution of the percentage of isolates that form strong (>0.240), moderate (0.120–0.240), and weak or no (<0.120) biofilm formation based on measuring optical density.

biofilm-forming ability and drug resistance among the strains studied. All 91 clinical *A. baumannii* isolates were MDR, and simultaneously exhibited robust biofilm formation, which is associated with enhanced resistance to multiple antibiotics. The majority of these isolates demonstrated complete resistance to β-lactam antibiotics, including carbapenems, indicating that biofilm formation may contribute to the persistence of infections and complicate treatment options. This finding aligns with existing literature suggesting that biofilm-embedded bacteria possess increased tolerance to antimicrobial agents, thereby facilitating chronic infections. For instance, Al-Hadethi and Turki (2022) [52] reported that all 60 *A. baumannii* isolates recovered from four hospitals in Iraq were capable of biofilm production, with 86.6% exhibiting moderate biofilm formation. In their study, a high proportion of isolates were resistant to ciprofloxacin, imipenem, and meropenem, and 58.3% and 31.6% of the isolates were classified as multidrug-resistant and extensively drug-resistant, respectively.

Similarly, a pilot study conducted in Karachi demonstrated that 100% of *A. baumannii* isolates were multidrug resistant, with 74.4% displaying a high multiple antibiotic resistance index (MARi 0.875–1.0). Among these, 27 isolates exhibited biofilm-forming ability, and a moderate positive correlation was observed between biofilm formation and MARi values, suggesting a potential role of biofilm formation in enhancing persistence and pathogenicity [53].

3.4. Prevalence of β-lactamase-related genes

The prevalence of β-lactamase encoding genes, including ESBLs, AmpC β-lactamases, and carbapenemases, was investigated in 30 MDR

Table 3
Prevalence and distribution of β-lactamase–encoding genes among MDR *A. baumannii* isolates (n = 30).

β-lactamase category	Gene	No. of positive isolates, n (%)
ESBL genes	*bla* $_{CTX}$	13 (43.3)
	bla $_{TEM}$	10 (33.3)
	bla $_{SHV}$	11 (36.6)
Carbapenemase genes	*bla* $_{OXA-48}$	21 (70)
	bla $_{VIM}$	15 (50)
	bla $_{IPM}$	9 (30)
	bla $_{NDM}$	12 (40)
	bla $_{KPC}$	2 (6.6)
AmpC genes	*bla* $_{DHA}$	4 (13.3)
Multiple gene carriage	≥2 β-lactamase genes	15 (50.0)

Differences in the distribution of β-lactamase gene categories among MDR *A. baumannii* isolates were assessed using the chi-square (χ^2) test; $p = 0.01$ was considered statistically significant.

A. baumannii isolates (Table 3). One or more β-lactamase genes were detected in all tested isolates. Among ESBL-associated genes, *bla* $_{CTX}$ was the most prevalent (56.6%), followed by *bla* $_{SHV}$ (53.3%) and *bla* $_{TEM}$ (26.6%). The predominance of *bla* $_{CTX}$ among ESBL-producing isolates is illustrated in Table 3 and Fig. 2.

AmpC β-lactamase genes were detected at a lower frequency, with *bla* $_{DHA}$ identified in 13.3% (4/30) of isolates. In contrast, none of the examined MDR *A. baumannii* isolates carried *bla* $_{CY1}$ or *bla* $_{CY2}$, suggesting a limited contribution of these AmpC variants in the study population.

Carbapenemase-encoding genes were widely distributed among the isolates. The most frequently detected carbapenemase gene was *bla* $_{OXA-48}$, identified in 70% (21/30) of isolates, followed by *bla* $_{VIM}$ (50%; 15/30), *bla* $_{NDM}$ (40%; 12/30), *bla* $_{IMP}$ (30%; 9/30), and *bla* $_{KPC}$ (6.6%; 2/30) (Table 3; Fig. 2). The high prevalence of *bla* $_{OXA-48}$ supports previous reports indicating that class D carbapenemases are among the most commonly detected enzymes in carbapenem-resistant *A. baumannii* [54,55].

Notably, 50% (15/30) of the carbapenemase-positive isolates harbored multiple carbapenemase genes, ranging from two to four per isolate, highlighting the extensive accumulation of resistance determinants. Statistical analysis revealed a significant association between β-lactamase gene category and the number of positive MDR *A. baumannii* isolates ($p < 0.01$) (Table 3). The coexistence of multiple resistance genes is often facilitated by transmissible genetic elements, such as plasmids and integrons, which frequently carry additional resistance determinants and further restrict available therapeutic options [54].

The rapid dissemination of carbapenemase-producing *A. baumannii* has been reported globally, including in Lebanon, Italy, and the United States [54,56]. Carbapenems are commonly regarded as last-resort agents for the treatment of severe infections caused by MDR *A. baumannii*; however, resistance to this antibiotic class has increased markedly over the past decade, particularly in nosocomial settings [57].

In addition to carbapenemase production, carbapenem resistance may arise through alternative or complementary mechanisms, including overproduction of ESBLs or AmpC β-lactamases in combination with porin loss or mutations that reduce outer membrane permeability, as well as the activation of multidrug efflux pumps under antibiotic selective pressure [58]. The improper or excessive use of carbapenems and third-generation cephalosporins has further accelerated the selection and spread of carbapenem resistance genes among Enterobacteriaceae and non-lactose-fermenting Gram-negative bacilli [59]. Moreover, plasmids encoding carbapenemases often harbor co-resistance genes to both β-lactam and non-β-lactam antibiotics, thereby promoting multidrug resistance and complicating treatment strategies [60].

3.5. Biosynthesis and physiochemical characterization of AgNPs

All five *C. farmeri* isolates were initially screened for their ability to biosynthesize AgNPs. Among these, only strain A121 demonstrated efficient nanoparticle synthesis and was therefore selected for subsequent physicochemical characterization.

3.5.1. Sequencing analysis of the 16S rRNA gene of C. farmeri A121

Comparative sequence BLASTn analysis against the NCBI GenBank revealed that strain A121 exhibited >99–100% sequence similarity with reference sequences of *C. farmeri*. The GenBank accession number assigned to the 16S rDNA sequence generated during this investigation is ON678253. To further validate the taxonomic placement of strain A121, phylogenetic analysis was performed using representative sequences of closely related *Citrobacter species* retrieved from GenBank. The phylogenetic tree was constructed with *Escherichia coli* designated as the outgroup to provide evolutionary context. As illustrated in Fig. 3, strain A121 clustered robustly within the *C. farmeri* clade, clearly separated from other *Citrobacter species*, thereby confirming its species-

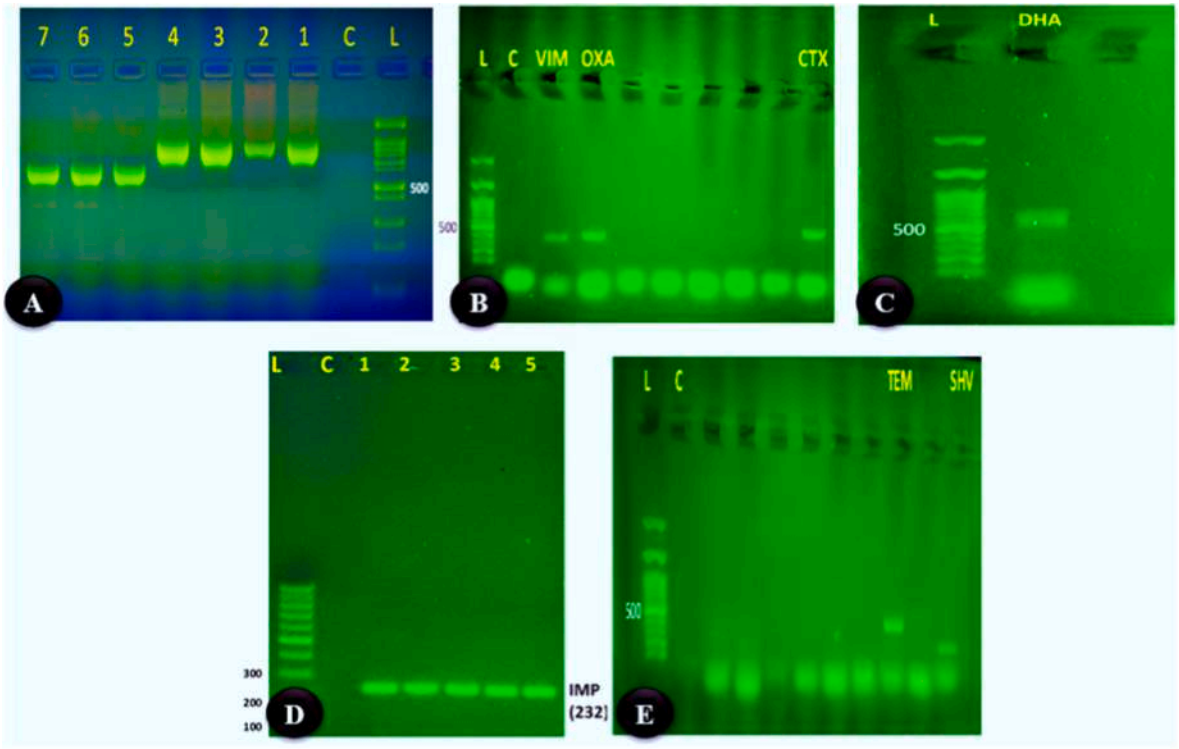

Fig. 2. Agarose gel electrophoresis of PCR amplicons showing the detection of β-lactamase encoding genes in multidrug-resistant *A. baumannii* isolates. **(A)** Amplification of carbapenemase genes bla_KPC (621 bp; lanes 1-4) and bla_NDM (621 bp; lanes 5-7). **(B)** Detection of bla_VIM (390 bp), bla_OXA-48 (438 bp), and bla_CTX (593 bp) genes. **(C)** Amplification of the AmpC gene bla_DHA (522 bp). **(D)** Detection of the carbapenemase gene bla_IMP. (**E**) Amplification of ESBL genes bla_TEM (445 bp) and bla_SHV (237 bp). Lane M represents the 1 kb DNA ladder, and lane C denotes the negative control.

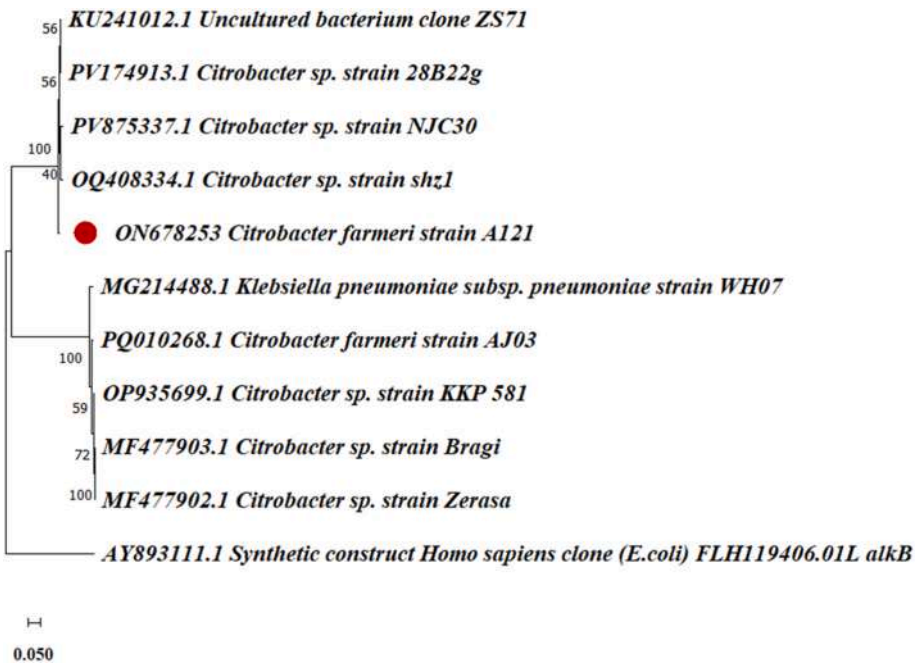

Fig. 3. Phylogenetic tree was constructed of *C. farmeri* A121 using the Neighbor-Joining method with 1000 bootstrap replicates. Evolutionary distances were calculated using the p-distance model. The analysis included 11 nucleotide sequences, with gaps and missing data removed (complete deletion), resulting in 104 positions in the final dataset. The tree was generated using MEGA11.

level identity.

The confirmed identification of strain A121 as *C. farmeri* is particularly relevant given that members of the genus *Citrobacter* are known to possess diverse metabolic capabilities, including metal ion reduction and nanoparticle biosynthesis [61,62]. Establishing precise taxonomic identity strengthens the reproducibility and scientific validity of subsequent analyses involving biosynthesized AgNPs. Moreover, accurate strain characterization is crucial when considering biosafety, pathogenic potential, and translational applications in antimicrobial research.

3.5.2. UV-visible spectroscopic analysis of AgNPs

The formation and stability of biosynthesized AgNPs were monitored using UV-visible spectroscopy. Within 24 h of incubation of the *C. farmeri* A121 culture supernatant with $AgNO_3$, a visible color change from pale yellow to dark brown was observed, indicating the reduction of Ag^+ ions and the formation of AgNPs. In contrast, the control reaction lacking bacterial biomass showed no discernible color change under identical conditions (Fig. 4A).

UV-visible absorption spectra recorded in the range of 300-800 nm revealed a single, well-defined absorption peak at approximately 405 nm, which is characteristic of the surface plasmon resonance (SPR) of colloidal silver nanoparticles [36]. The appearance of a solitary SPR peak suggests the formation of predominantly spherical AgNPs [63]. UV-visible spectroscopy remains a widely employed and reliable technique for the preliminary structural characterization of metallic nanoparticles [11].

The biosynthesis of AgNPs using *C. farmeri* represents an environmentally benign and cost-effective approach, offering advantages such as low energy input, enhanced biocompatibility, and controlled crystal growth compared to conventional physicochemical methods [12]. Microbial systems are recognized as efficient sources of reducing and stabilizing agents, facilitating nanoparticle synthesis under mild conditions [64]. In the present study, the UV spectra further exhibited a cut-off wavelength at 316 nm, consistent with earlier reports on biologically synthesized AgNPs [65], thereby confirming successful nanoparticle formation.

3.5.3. XRD analysis of AgNPs

XRD analysis was performed to determine the crystalline nature and phase purity of the biosynthesized AgNPs. The diffraction pattern displayed distinct Bragg reflections at 2θ values of 38.037°, 44.205°, and 64.344°, corresponding to the (111), (200), and (220) crystallographic planes of face-centered cubic (fcc) silver, respectively (Fig. 4B). These diffraction peaks were in good agreement with the standard silver diffraction data (JCPDS file no. 98-018-0878) (Table 4), confirming the crystalline structure of the nanoparticles.

A slight leftward shift of the dominant (111) peak from the standard value (38.116°) to 38.037° was observed, which may be attributed to lattice expansion arising from size-dependent effects, crystal strain, or thermally induced atomic vibrations during nanoparticle formation. An increase in interplanar spacing (d-spacing), as explained by Bragg's law, results in peak shifts toward lower 2θ values [66,67]. Similar peak shifts have been reported previously for AgNPs synthesized via alternative green routes, including sol–gel methods using ascorbic acid as a reducing agent [68], where such deviations were linked to nanoparticle size and surface effects.

The average crystallite size (ACS) of the AgNPs synthesized by *C. farmeri* A121 was estimated using the Scherrer equation:

$$D = \frac{k\lambda}{\beta \cos \theta} \cdots \quad (1)$$

where D represents the average crystallite size, k is the shape factor (0.9), λ is the X-ray wavelength (1.54 Å), β denotes the full width at half maximum (FWHM), and θ is the Bragg angle. Based on this calculation, the ACS of the biosynthesized AgNPs was determined to be approximately 51.73 nm, corroborating their nanocrystalline nature.

3.5.4. Fouriertransform-infrared (FT-IR) analysis of AgNPs

FT-IR spectroscopy was employed to identify the functional groups involved in the reduction of silver ions and the subsequent stabilization and capping of the biosynthesized AgNPs (Fig. 4C). The FT-IR spectrum exhibited three prominent absorption bands at 3252.36, 1636.30, and 405.94 cm^{-1}, corresponding to distinct vibrational modes of biomolecular functional groups associated with nanoparticle formation.

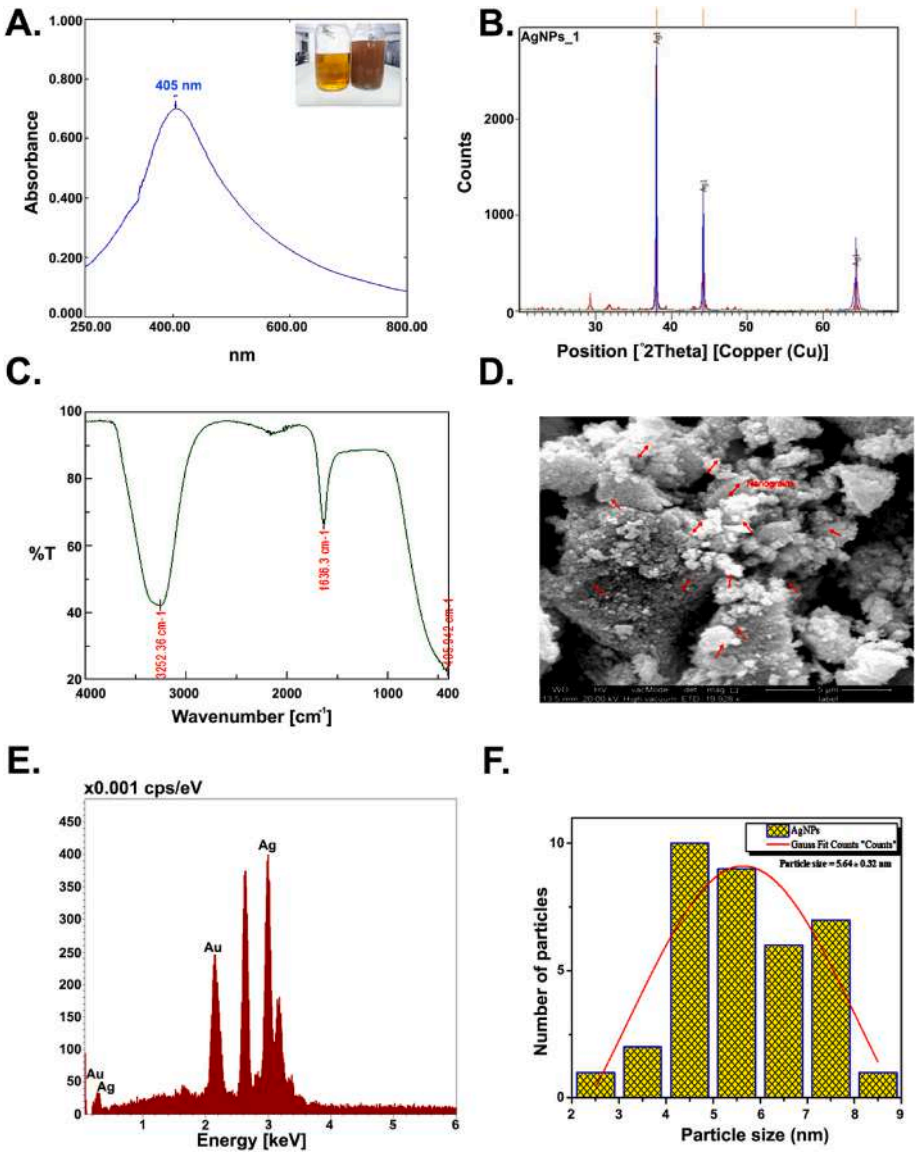

Fig. 4. Characterization of biosynthesized AgNPs. (A) Visual color change of the reaction mixture and corresponding UV–visible absorption spectrum confirming AgNP formation. (B) XRD pattern showing the crystalline nature of AgNPs. (C) FT-IR spectrum indicating functional groups involved in nanoparticle reduction and stabilization. (D) FE-SEM micrographs illustrating the surface morphology of AgNPs. (E) EDS spectrum confirming the elemental composition of silver. (F) TEM images showing the size and morphology of the synthesized AgNPs.

Table 4
X-ray diffraction (XRD) peak parameters of biosynthesized silver nanoparticles (AgNPs), indexed and matched with the standard face-centered cubic silver reference pattern (JCPDS card no. 98-018-0878).

2θ position (°)	Peak intensity counts (°)	FWHM (°)	Interplanar spacing, d (Å)	Relative Intensity (%)	Tip Width	JCPDS reference
38.037	2898.09	0.096	2.36379	100.00	0.1152	98-018-0878
44.205	1137.58	0.192	2.04722	39.25	0.2304	98-018-0878
64.345	354.45	0.576	1.44666	12.23	0.6912	98-018-0878

The broad absorption band observed at 3252.36 cm^{-1} is attributed to the stretching vibrations of C–O functional groups, typically associated with alcohols and phenolic compounds, which are known to act as reducing agents during nanoparticle biosynthesis [69]. The peak at 1636.30 cm^{-1} corresponds to out-of-plane bending of C=C bonds and the stretching vibrations of carbonyl (C=O) groups, commonly found in ketones and aldehydes, with transmittance intensities ranging from 60 to 80% [70,71]. These functional groups are frequently implicated in electron donation processes that facilitate the reduction of Ag^{+} to Ag^{0}.

Additionally, the absorption band detected at 405.94 cm^{-1} is characteristic of silver-oxygen or silver ionic (Ag^{+}) interactions, indicating the presence and stabilization of silver species within the nanoparticle matrix [72]. Collectively, these results suggest that biomolecules associated with the bacterial cell envelope play a dual role in both the reduction of silver ions and the stabilization of the resulting nanoparticles. Such biomolecules act as natural capping agents, facilitating nucleation and preventing excessive aggregation of AgNPs, as reported in earlier studies [73].

3.5.5. Morphology and shape of silver nanoparticles

3.5.5.1. Field emission scanning electron microscopy (FE-SEM). FE-SEM analysis revealed that the biosynthesized AgNPs predominantly exhibited quasi-spherical to spherical morphologies, with a tendency to form irregular aggregates (Fig. 4D). The pronounced intensity of the (111) diffraction peak observed in the XRD analysis further supports isotropic crystallite growth, a characteristic feature of spherical silver nanoparticles. SEM micrographs showed clustered spherical nanograins, which is consistent with earlier reports on biologically synthesized AgNPs [9,74].

The observed aggregation and flaky structures are likely attributable to the high surface energy of nanoparticles formed in aqueous environments, which promotes interparticle interactions during biosynthesis [75].

Elemental composition analysis using FE-SEM coupled with energy-dispersive X-ray spectroscopy (EDS) revealed a strong and characteristic signal at approximately 3 keV, confirming the presence of elemental silver (Fig. 4E). This finding corroborates previous studies demonstrating the successful bacterial synthesis of AgNPs [76]. A minor peak corresponding to gold (Au) was also detected in the EDS spectrum, which may be attributed to sample preparation artifacts or contamination during mounting, as previously reported by Gurtu and Bakshi (2018) [77].

3.5.5.2. Transmission electron microscopy (TEM). Transmission electron microscopy was employed to obtain detailed insights into nanoparticle morphology and size distribution. TEM images revealed a population of predominantly spherical, well-separated, and relatively uniform AgNPs (Fig. 4F). Quantitative analysis of TEM micrographs using ImageJ software indicated an average particle size of 5.64 ± 0.32 nm. The corresponding size distribution histogram suggested a degree of polydispersity, which is commonly observed in biologically synthesized nanoparticles due to variations in nucleation and growth kinetics [78].

These observations are consistent with previous reports describing bacterial synthesis of spherical and occasionally aggregated AgNPs [16,79]. Notably, the particle sizes determined by TEM were smaller than the crystallite sizes estimated from XRD analysis. This discrepancy can be attributed to nanoparticle agglomeration effects inherent to XRD measurements, where coherently aligned crystalline domains within agglomerated particles contribute to an apparent increase in crystallite size. In contrast, TEM provides direct visualization of individual nanoparticles, yielding more accurate estimates of primary particle size [80].

3.6. Antimicrobial activity of biosynthesized AgNPs against MDR *A. baumannii*

The antibacterial efficacy of biosynthesized AgNPs from A121 strain against MDR *A. baumannii* (91 isolates), was evaluated using the disc diffusion assay at three concentrations (1.25, 2.5, and 5 mg/mL). The AgNPs exhibited a concentration-dependent inhibitory effect, with zones of inhibition ranging from 10 to 13 mm at 1.25 mg/mL, 12-14 mm at 2.5 mg/mL, and 15-17 mm at 5 mg/mL (Table 5; **Figure SP1).** The progressive increase in inhibition zones with rising AgNP concentrations indicates enhanced antibacterial activity at higher doses.

These findings demonstrate that biosynthesized AgNPs possess pronounced antibacterial activity against MDR *A. baumannii*, with efficacy strongly influenced by nanoparticle concentration. Similar concentration-dependent antibacterial effects of AgNPs against *A. baumannii* and other clinically relevant pathogens have been previously reported, underscoring the broad-spectrum potential of biologically synthesized AgNPs as alternative antimicrobial agents [42,81,82].

Table 5
Antibacterial activity of biosynthesized silver nanoparticles (AgNPs) against multidrug-resistant *A. baumannii*, expressed as zones of inhibition (mm) determined by the disc diffusion assay at different AgNP concentrations.

MDR *A. baumannii*	Different AgNP concentrations used		
	1.25 mg/mL	2.5 mg/mL	5 mg/mL
Zones of Inhibition (mm)	10-13	12-14	15-17

The antibacterial mechanism of AgNPs is multifactorial. One of the primary modes of action involves the sustained release of Ag^{+} ions, which interact with thiol (-SH) groups of bacterial proteins and enzymes, leading to their inactivation and subsequent disruption of cell membrane integrity. Following membrane damage, Ag^{+} ions can penetrate the bacterial cytoplasm and interact with genomic DNA by intercalating between purine and pyrimidine base pairs, thereby disrupting hydrogen bonding, inhibiting DNA replication, and ultimately impairing cell division [83,84].

Gram-negative bacteria such as *A. baumannii* are particularly susceptible to AgNPs due to the negatively charged components of their outer membrane, which promote electrostatic interactions with positively charged biosynthesized nanoparticles. This enhanced adhesion facilitates nanoparticle uptake and contributes to the broad antibacterial effectiveness of AgNPs, irrespective of existing antimicrobial resistance profiles [13]. In addition, interactions between microorganisms and metal-based nanoparticles induce oxidative stress through the generation of reactive oxygen species (ROS), leading to oxidative damage of cellular components and bacterial cell death [85].

Importantly, AgNPs have also been reported to interfere with efflux pump systems, a key resistance mechanism employed by MDR *A. baumannii*. Inhibition of efflux activity, as evidenced by reduced ethidium bromide (EtBr) efflux, may occur either through direct binding of AgNPs to efflux pump active sites or through disruption of the energy-dependent efflux process. This interference results in increased intracellular accumulation of antimicrobial agents, thereby enhancing bacterial susceptibility [86].

3.7. Antibiofilm activity of AgNPs

The antibiofilm efficacy of the biosynthesized AgNPs from A121 strain was evaluated against all (60) biofilm producing MDR *Acinetobacter baumannii* using a microtiter plate assay following 24 h of incubation. All tested isolates were exposed to increasing concentrations of AgNPs ranging from 19.531 to 2500 μg/mL, and biofilm biomass was quantified relative to untreated controls (Fig. 5). The results demonstrated a clear, concentration-dependent inhibition of biofilm formation by AgNPs. Specifically, biofilm biomass was reduced by 38%, 40%, 53%, 60%, 72%, 85%, 91%, and 95% at AgNP concentrations of 19.531, 39.0625, 78.125, 156.25, 312.5, 625, 1250, and 2500 μg/mL, respectively, compared with control cultures. Statistical analysis confirmed that the antibiofilm activity of AgNPs was highly significant ($p < 0.001$).

The most pronounced antibiofilm effects were observed at AgNP concentrations of 2500 and 1250 μg/mL, achieving biofilm inhibition of 95% and 91%, respectively. These findings indicate that biosynthesized AgNPs are capable of effectively disrupting established biofilms of MDR *A. baumannii* at concentrations that are potentially achievable in clinical and biomedical applications. Similar observations have been reported by Hetta et al. (2021a) [42], who demonstrated rapid detachment and suppression of *A. baumannii* biofilms following exposure to AgNPs.

The antibiofilm activity of metal-based nanoparticles has been attributed to their ability to penetrate the dense extracellular polymeric substance (EPS) matrix, a defining feature of mature biofilms that confers resistance to antimicrobial agents. Metallic nanoparticles, including AgNPs, possess nanoscale dimensions that facilitate their diffusion through biofilm layers, thereby impairing bacterial adhesion and biofilm stability [87]. Consistent with the present findings, several studies have reported significant reductions in bacterial biofilm biomass at concentrations corresponding to the minimum inhibitory concentrations of AgNPs [42,88].

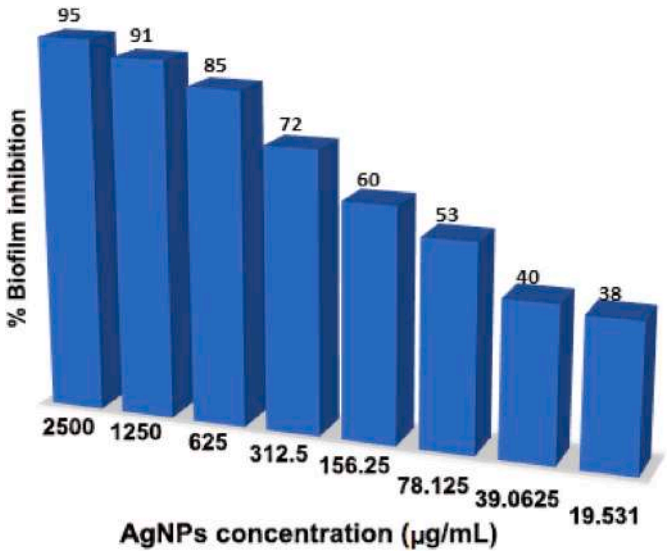

Fig. 5. Concentration-dependent antibiofilm activity of biosynthesized silver nanoparticles (AgNPs) against a strong biofilm-producing *Acinetobacter baumannii* isolate. The percentage inhibition of biofilm formation was quantified relative to the untreated control following exposure to increasing concentrations of AgNPs.

Furthermore, AgNP-mediated inhibition of biofilm formation has been linked to interference with quorum sensing pathways and disruption of EPS synthesis. Mohanta et al. (2023) [89] demonstrated that silver nanocomposites reduced biofilm roughness in *A. baumannii* by targeting quorum sensing-associated virulence factors. Sheng et al. (2022) [15] also reported approximately 50% reduction in biofilm formation in both Gram-negative and Gram-positive bacteria upon exposure to AgNPs. Mechanistically, AgNPs and the released Ag^{+} ions can bind to cysteine residues in biofilm-associated proteins, leading to protein denaturation and suppression of EPS production, ultimately destabilizing the biofilm architecture [90].

4. Conclusions

This study demonstrates the successful biosynthesis of AgNPs using *C. farmeri* and provides a comprehensive evaluation of their antibacterial and antibiofilm efficacy against MDR *A. baumannii*. A total of 91 clinical MDR *A. baumannii* isolates were recovered from diverse clinical specimens, with sputum representing the predominant source, reflecting the clinical burden of respiratory tract infections caused by this pathogen. The demographic analysis revealed a higher prevalence of infection among male patients, particularly within the economically active age group of 20-60 years, highlighting a population at increased risk of MDR *A. baumannii* infection.

Antimicrobial susceptibility profiling revealed extensive resistance across multiple clinically relevant antibiotic classes, including penicillins, cephalosporins, and carbapenems, underscoring the limited therapeutic options currently available for the treatment of *A. baumannii* infections. The strong biofilm-forming capacity observed in the majority of isolates further emphasizes the clinical challenge posed by this pathogen, as biofilm formation contributes to persistence, immune evasion, and antimicrobial tolerance. Molecular characterization confirmed a high prevalence of β-lactamase-encoding genes, with bla_OXA-48 emerging as the dominant carbapenemase determinant, consistent with global reports highlighting the dissemination of class D carbapenemases among MDR *A. baumannii* strains.

Physicochemical characterization confirmed the successful formation of predominantly spherical AgNPs with an average crystallite size of 51.73 nm. Spectroscopic analyses indicated that bacterial biomolecules, particularly carbonyl-containing functional groups such as aldehydes and ketones, played a critical role in the reduction, stabilization, and surface functionalization of the nanoparticles. These surface-associated biomolecules are likely to enhance nanoparticle stability and biological activity.

Functionally, the biosynthesized AgNPs exhibited pronounced antibacterial activity against MDR *A. baumannii*, with inhibition zones reaching 15-17 mm at the highest tested concentration (5 mg/mL). Moreover, a strong concentration-dependent inhibition of biofilm formation was observed, demonstrating the ability of AgNPs to disrupt one of the most critical virulence and resistance mechanisms of *A. baumannii*. Collectively, these findings indicate that biologically synthesized AgNPs represent a promising alternative or adjunctive strategy to conventional antibiotics for combating MDR *A. baumannii*, particularly in the context of biofilm-associated infections.

5. Future recommendations

To advance the translational potential of biosynthesized AgNPs, further investigations are warranted. First, detailed cytotoxicity and biocompatibility assessments using relevant human cell lines and *in vivo* models are essential to define a safe therapeutic window. Second, mechanistic studies focusing on nanoparticle-cell interactions, biofilm disruption pathways, and efflux pump inhibition will provide deeper insights into the mode of action of AgNPs. Third, evaluation of synergistic effects between AgNPs and conventional antibiotics may reveal combination strategies capable of restoring antibiotic efficacy at lower doses. Additionally, in combination with disc-diffusion assay, researchers should add checkerboard microdilution method and time-kill assays for further validation. Moreover, viable bacterial counting methods will use in future studies to more accurately assess live and dead cells within the biofilm, considering that biofilms comprise both bacterial cells and an extracellular matrix. Finally, *in vivo* infection models and formulation-based delivery approaches should be explored to assess the clinical applicability of AgNPs for the management of MDR and biofilm-associated *A. baumannii* infections.

Consent for publication

Not applicable.

Ethical approval

This study was reviewed and approved by the Ethics Committee of the College of Pharmacy, Hawler Medical University (Approval No. 2022AN0292). The requirement for written informed consent was waived by the committee. All experimental procedures were conducted in accordance with relevant institutional guidelines and applicable regulations.

Funding

No funds available.

CRediT authorship contribution statement

Sazan Moffaq Abdulaziz: Data curation, Formal analysis, Writing – original draft. **Sayran H. Haji:** Supervision, Writing – original draft, Writing – review & editing. **Aryan R. Ganjo:** Conceptualization, Supervision, Writing – original draft. **Safaa Toma Hanna Aka:** Writing – original draft. **Nidhi Bhardwaj:** Data curation, Formal analysis, Writing – original draft. **Indu Bhardwaj:** Data curation, Formal analysis, Writing – original draft. **Soumya Ghosh:** Data curation, Formal analysis, Supervision, Writing – original draft, Writing – review & editing.

Declaration of competing interest

The authors declare that they have no known competing financial interests or personal relationships that could have appeared to influence the work reported in this paper.

Acknowledgements

Not applicable.

Appendix A. Supplementary data

Supplementary data to this article can be found online at https://doi.org/10.1016/j.micpath.2026.108580.

Data availability

Data will be made available on request.

References

[1] T.S. Mohamad, J.K. Rahman, A.A. Ahmed, A.R. Ganjo, Down-regulation of abaI, abaR, Bap and OmpA genes in Acinetobacter baumannii by ethanol extract of Glycyrrhiza glabra after toxicity assessment: downregulation of quorum sensing genes in A. baumannii, Cell. Mol. Biol. 69 (2023) 194–200.
[2] S. Roy, G. Chowdhury, A.K. Mukhopadhyay, S. Dutta, S. Basu, Convergence of biofilm formation and antibiotic resistance in Acinetobacter baumannii infection, Front. Med. 9 (2022) 793615.
[3] F.P. Dsouza, S. Dinesh, S. Sharma, Understanding the intricacies of microbial biofilm formation and its endurance in chronic infections: a key to advancing biofilm-targeted therapeutic strategies, Arch. Microbiol. 206 (2024) 85.
[4] J.K. Rahman, A.A. Ahmed, A.R. Ganjo, T.S. Mohamad, Assessment of toxicity, anti-quorum sensing and anti-biofilm production effects of Hypericum triquetrifolium turra extract on multi-drug resistant Acinetobacter baumannii, J. King Saud Univ. Sci. 35 (2023) 102714.
[5] P.-W. Su, E.C. Yang, S.-H. Moi, C.-H. Yang, L.-Y. Chuang, Prevalence of carbapenem resistance genes among Acinetobacter baumannii isolated from a teaching hospital in Taiwan, Antibiotics 12 (2023) 1357.
[6] A.R. Ganjo, D.M. Maghdid, I.Y. Mansoor, D.J. Kok, J.A. Severin, H.A. Verbrugh, et al., OXA-carbapenemases present in clinical Acinetobacter baumannii-calcoaceticus complex isolates from patients in Kurdistan region, Iraq. Microbial drug resistance 22 (2016) 627–637.
[7] E.E. Heba, N. Islam, N. Nehad, S. Basma, A.-H. Hesham, Z. Mayada, et al., Molecular characterization of carbapenem resistant Gram-negative rods in neonatal intensive care unit of mansoura university childrens hospital, Afr. J. Microbiol. Res. 15 (2021) 286–294.
[8] H.S. Elbadawi, K. Elhag, E. Mahgoub, H.N. Altayb, M.M.A. Hamid, Prevalence and Molecular Characterization of Carbapenem Resistance Gram Negative Bacilli Among Hospitalized Patients in Khartoum State, 2019.
[9] S.H. Haji, F.A. Ali, S.T.H. Aka, Synergistic antibacterial activity of silver nanoparticles biosynthesized by carbapenem-resistant Gram-negative Bacilli, Sci. Rep. 12 (2022) 15254.
[10] H.F. Hetta, Y.N. Ramadan, A.I. Al-Harbi, A, E. Ahmed, B. Battah, N.H. Abd Ellah, et al., Nanotechnology as a promising approach to combat multidrug resistant bacteria: a comprehensive review and future perspectives, Biomedicines 11 (2023) 413.
[11] M. Wypij, J. Czarnecka, M. Świecimska, H. Dahm, M. Rai, P. Golinska, Synthesis, characterization and evaluation of antimicrobial and cytotoxic activities of biogenic silver nanoparticles synthesized from Streptomyces xinghaiensis OF1 strain, World J. Microbiol. Biotechnol. 34 (2018) 1–13.
[12] K. Vadakkan, N.P. Rumjit, A.K. Ngangbam, S. Vijayanand, N.K. Nedumpillil, Novel advancements in the sustainable green synthesis approach of silver nanoparticles (AgNPs) for antibacterial therapeutic applications, Coord. Chem. Rev. 499 (2024) 215528.
[13] A.R. Alnsour, R.M. Daghmash, M.M. Masadeh, K.H. Alzoubi, M.M. Masadeh, N. H. Bataineh, et al., The pharmaceutical role of silver nanoparticles in treating multidrug-resistant bacteria and biofilms, Curr. Nanosci. 20 (2024) 471–494.
[14] A.J. Siddiqui, M. Patel, S. Jahan, A. Abdelgadir, M.J. Alam, M.M. Alshahrani, et al., Silver nanoparticles derived from probiotic Lactobacillus casei—A novel approach for combating bacterial infections and cancer, Probiotics Antimicrob. Proteins 17 (2025) 1277–1294.
[15] Y. Sheng, M. Narayanan, S. Basha, A. Elfasakhany, K. Brindhadevi, C. Xia, et al., In vitro and in vivo efficacy of green synthesized AgNPs against gram negative and gram positive bacterial pathogens, Process Biochem. 112 (2022) 241–247.
[16] S. Raj, R. Trivedi, V. Soni, Biogenic synthesis of silver nanoparticles, characterization and their applications—a review, Surfaces 5 (2021) 67–90.
[17] A.C.C. Santos, J.L. Corrêa, R.C. Cerqueira, G.C. Batista, T.S. Rodrigues, L.M. M. Bernardes, et al., Microbial synthesis of silver nanoparticles using bacterial supernatants from Brazilian stingless bees with antimicrobial activity, Sci. Rep. (2026).
[18] I. Bhardwaj, N. Bhardwaj, V. Kumar, S. Kumari, K. Dulta, J. Aman, et al., Synergistic effects of bacillus cereus Mn-5 PGPR-Derived silver oxide nanoparticles on tomato plant growth, stress resilience and nutritional enhancement, J. Sustain. Agric. Environ. 4 (2025) e70090.
[19] M.G. Al-Asbahi, B.A. Al-Ofiry, F.A. Saad, A. Alnehia, M.Q. Al-Gunaid, Silver nanoparticles biosynthesis using mixture of Lactobacillus sp. and bacillus sp. growth and their antibacterial activity, Sci. Rep. 14 (2024) 10224.
[20] M. Guilger-Casagrande, Rd Lima, Synthesis of silver nanoparticles mediated by fungi: a review, Front. Bioeng. Biotechnol. 7 (2019) 287.
[21] M. Anzum, A. Molla, A. Islam, H. Akhter, A. Al Moyeen, R. Zaman, et al., Green nanotechnology: adenanthera pavonina-derived silver nanoparticles with antibacterial and photocatalytic properties, Sci. Rep. (2026).
[22] S.A. Al-Audah, A.I. Alghamdi, S.I. Alsanie, N.M. Alabdalla, A. Alawdah, N. Alenezi, et al., Green synthesis of silver nanoparticles with antibacterial, anti-inflammatory, and antioxidant activity using Convolvulus arvensis, Int. J. Mol. Sci. 27 (2026) 1210.
[23] M. Alavi, Bacteria and fungi as major bio-sources to fabricate silver nanoparticles with antibacterial activities, Expert Rev. Anti-infect. Ther. 20 (2022) 897–906.
[24] H. Kollenda, H. Frickmann, R. Ben Helal, D.F. Wiemer, H. Naija, M.S. El Asli, et al., Screening for carbapenemases in ertapenem-resistant enterobacteriaceae collected at a Tunisian hospital between 2014 and 2018, Eur J Microbiol Immunol (Bp) 9 (2019) 9–13.
[25] K.H. Ibrahem, S.M. Abdulaziz, S.H. Haj, A.R. Ganjo, N. Bhardwaj, I. Bhardwaj, et al., Biosynthesized gold nanoparticles from proteus mirabilis: a synergistic strategy against multidrug-resistant gram-negative bacteria, Microb. Pathog. (2025) 108178.
[26] K.K. Ghaima, S.M.K. Saadedin, K.A. Jassim, Isolation, molecular identification and antimicrobial susceptibility of Acinetobacter baumannii isolated from Baghdad hospitals, Burns 27 (2015) 31.
[27] S.F. Altschul, T.L. Madden, A.A. Schäffer, J. Zhang, Z. Zhang, W. Miller, et al., Gapped BLAST and PSI-BLAST: a new generation of protein database search programs, Nucleic Acids Res. 25 (1997) 3389–3402.
[28] K. Tamura, G. Stecher, S. Kumar, MEGA11: molecular evolutionary genetics analysis version 11, Mol. Biol. Evol. 38 (2021) 3022–3027.
[29] N. Saitou, M. Nei, The neighbor-joining method: a new method for reconstructing phylogenetic trees, Mol. Biol. Evol. 4 (1987) 406–425.
[30] J. Felsenstein, Confidence limits on phylogenies: an approach using the bootstrap, Evolution 39 (1985) 783–791.
[31] M. Nei, S. Kumar, Molecular Evolution and Phylogenetics, Oxford University Press, 2000.
[32] M. Peiris, S. Fernando, P. Jayaweera, N. Arachchi, T. Guansekara, Comparison of antimicrobial properties of silver nanoparticles synthesized from selected bacteria, Indian J. Microbiol. 58 (2018) 301–311.
[33] M. Khaleghi, S. Khorrami, H. Ravan, Identification of Bacillus thuringiensis bacterial strain isolated from the mine soil as a robust agent in the biosynthesis of silver nanoparticles with strong antibacterial and anti-biofilm activities, Biocatal. Agric. Biotechnol. 18 (2019) 101047.
[34] C. Singh, A. Singh, S. Kumar, M. Kumar, P. Sharma, D. Majumdar, Development and validation of different ultraviolet-spectrophotometric methods for the estimation of besifloxacin in different simulated body fluids, Indian J. Pharmaceut. Sci. 77 (2015) 399.
[35] M.A. Shaker, M.I. Shaaban, Synthesis of silver nanoparticles with antimicrobial and anti-adherence activities against multidrug-resistant isolates from Acinetobacter baumannii, J. Taibah Univ. Med. Sci. 12 (2017) 291–297.
[36] R. Singh, P. Wagh, S. Wadhwani, S. Gaidhani, A. Kumbhar, J. Bellare, et al., Synthesis, optimization, and characterization of silver nanoparticles from Acinetobacter calcoaceticus and their enhanced antibacterial activity when combined with antibiotics, Int. J. Nanomed. 8 (2013) 4277.
[37] M.S. John, J.A. Nagoth, K.P. Ramasamy, A. Mancini, G. Giuli, A. Natalello, et al., Synthesis of bioactive silver nanoparticles by a pseudomonas strain associated with the antarctic psychrophilic protozoon Euplotes focardii, Mar. Drugs 18 (2020) 38.
[38] M. Gajdács, Z. Baráth, K. Kárpáti, D. Szabó, D. Usai, S. Zanetti, et al., No correlation between biofilm formation, virulence factors, and antibiotic resistance in pseudomonas aeruginosa: results from a laboratory-based in vitro study, Antibiotics 10 (2021) 1134.
[39] L. Poirel, T.R. Walsh, V. Cuvillier, P. Nordmann, Multiplex PCR for detection of acquired carbapenemase genes, Diagn. Microbiol. Infect. Dis. 70 (2011) 119–123.
[40] T. de Sousa, M. Hébraud, O. Alves, E. Costa, L. Maltez, J.E. Pereira, et al., Study of antimicrobial resistance, biofilm formation, and motility of Pseudomonas aeruginosa derived from urine samples, Microorganisms 11 (2023) 1345.
[41] S. Stepanović, D. Vuković, V. Hola, G.D. Bonaventura, S. Djukić, I. Ćirković, et al., Quantification of biofilm in microtiter plates: overview of testing conditions and practical recommendations for assessment of biofilm production by staphylococci, Apmis 115 (2007) 891–899.
[42] H.F. Hetta, I.M. Al-Kadmy, S.S. Khazaal, S. Abbas, A. Suhail, M.A. El-Mokhtar, et al., Antibiofilm and antivirulence potential of silver nanoparticles against multidrug-resistant Acinetobacter baumannii, Sci. Rep. 11 (2021) 10751.
[43] A. Barapatre, K.R. Aadil, H. Jha, Synergistic antibacterial and antibiofilm activity of silver nanoparticles biosynthesized by lignin-degrading fungus, Bioresour. Bioproces. 3 (2016) 1–13.
[44] Rahman J. Khidhr, Ahmed A. Ahmed, A.R. Ganjo, T. Salih Mohamad, Assessment of toxicity, anti-quorum sensing and anti-biofilm production effects of Hypericum triquetrifolium turra extract on multi-drug resistant Acinetobacter baumannii, J. King Saud Univ. Sci. 35 (2023) 102714.

[45] M. Al-Tamimi, H. Albalawi, M. Alkhawaldeh, A. Alazzam, H. Ramadan, M. Altalalwah, et al., Multidrug-resistant Acinetobacter baumannii in Jordan, Microorganisms 10 (2022) 849.
[46] M. Al-Tamimi, H. Albalawi, M. Alkhawaldeh, A. Alazzam, H. Ramadan, M. Altalalwah, et al., Multidrug-resistant Acinetobacter baumannii in Jordan, Microorganisms 10 (2022) 849.
[47] M. Rossitto, G. Vrenna, V. Tuccio Guarna Assanti, N. Essa, M.L. De Santis, A. Granaglia, et al., Identification of the bla OXA-23 gene in the first mucoid XDR Acinetobacter baumannii isolated from a patient with cystic fibrosis, J. Clin. Med. 12 (2023) 6582.
[48] E. Sheck, A. Romanov, V. Shapovalova, E. Shaidullina, A. Martinovich, N. Ivanchik, et al., Acinetobacter non-baumannii species: occurrence in infections in hospitalized patients, identification, and antibiotic resistance, Antibiotics 12 (2023) 1301.
[49] C. Jin, F. Zhou, Q. Cui, J. Qiang, C. An, Molecular characteristics of carbapenem-resistant Enterobacter cloacae in a tertiary hospital in China, Infect. Drug Resist. 13 (2020) 1575.
[50] D.P.M. Sethuvel, Y.D. Bakthavatchalam, M. Karthik, M. Irulappan, R. Shrivastava, H. Periasamy, et al., β-Lactam resistance in ESKAPE pathogens mediated through modifications in penicillin-binding proteins: an overview, Infect. Dis. Ther. 12 (2023) 829–841.
[51] A. Thacharodi, A. Vithlani, S. Hassan, A. Alqahtani, A. Pugazhendhi, Carbapenem-resistant Acinetobacter baumannii raises global alarm for new antibiotic regimens, iScience 27 (2024).
[52] J.S. Al-Hadethi, A.M. Turki, Antibiogram and biofilm-forming capacity of Acinetobacter baumannii isolated from anbar hospitals, Int. J. Health Sci. 6 (2022) 247–260.
[53] M. Zehra, S. Asghar, R. Ilyas, Y. Usmani, R.M.A. Khan, Z.A. Mirani, et al., Relationship of biofilm formation with antibiotic resistance, virulence determinants and genetic diversity in clinically isolated Acinetobacter baumannii strains in Karachi, Pakistan, Microb. Pathog. 200 (2025) 107283.
[54] S. Sabour, K. Bantle, A. Bhatnagar, J.Y. Huang, A. Biggs, J. Bodnar, et al., Descriptive analysis of targeted carbapenemase genes and antibiotic susceptibility profiles among carbapenem-resistant Acinetobacter baumannii tested in the antimicrobial resistance Laboratory Network—United States, 2017–2020, Microbiol. Spectr. (2024) e02828-23.
[55] X. Wang, H. Zhang, S. Yu, D. Li, M.R. Gillings, H. Ren, et al., Inter-plasmid transfer of antibiotic resistance genes accelerates antibiotic resistance in bacterial pathogens, ISME J. (2024) wrad032.
[56] D. Daaboul, S. Oueslati, M. Rima, I.I. Kassem, H. Mallat, A. Birer, et al., The emergence of carbapenemase-producing Enterobacterales in hospitals: a major challenge for a debilitated healthcare system in Lebanon, Front. Public Health 11 (2023).
[57] A. Corona, V. De Santis, A. Agarossi, A. Prete, D. Cattaneo, G. Tomasini, et al., Antibiotic therapy strategies for treating gram-negative severe infections in the critically ill: a narrative review, Antibiotics 12 (2023) 1262.
[58] M.A. AL-Salmi, Study of the Genetic Characteristics of Cephalosporins and Carbapenems-Resistant Bacteria on the Red Sea Coast in Jeddah, KING ABDULAZIZ UNIVERSITY JEDDAH, 2024.
[59] T.S. Kostyanev, Building a European Laboratory Network to Combat Bacterial Resistance by Boosting the Clinical Development of Anti-infectives, University of Antwerp, 2021.
[60] J.F. Ayala-Zavala, S.A. Ibrahim, T. Yang, M.S. Imam, K.A. El-Tarabily, M. El-Saadony, et al., Medicinal Plants as Alternative Antimicrobial Agents to Combating the multi-drug Resistant Human Pathogens: a Comprehensive Review, 2022.
[61] M.T. Matsena, S.M. Tichapondwa, E.M.N. Chirwa, Synthesis of biogenic palladium nanoparticles using citrobacter sp. for application as anode electrocatalyst in a microbial fuel cell, Catalysts 10 (2020) 838.
[62] M.H. AlKhafaji, R.H. Mohsin, M.J. Kadhim, Biosynthesis of iron oxide nanoparticles using food origin Citrobacter freundii in optimized conditions, Basrah J. Agricultural Sci. 37 (2024) 249–263.
[63] B. Das, S.K. Dash, D. Mandal, T. Ghosh, S. Chattopadhyay, S. Tripathy, et al., Green synthesized silver nanoparticles destroy multidrug resistant bacteria via reactive oxygen species mediated membrane damage, Arab. J. Chem. 10 (2017) 862–876.
[64] P.K. Dikshit, J. Kumar, A.K. Das, S. Sadhu, S. Sharma, S. Singh, et al., Green synthesis of metallic nanoparticles: applications and limitations, Catalysts 11 (2021) 902.
[65] M. Mahiuddin, P. Saha, B. Ochiai, Green synthesis and catalytic activity of silver nanoparticles based on Piper chaba stem extracts, Nanomaterials 10 (2020) 1777.
[66] M.A. Alam, R.K. Bishwas, S. Mostofa, S.A. Jahan, Impact on preferred orientation and crystal strain behavior of nanocrystal anatase-TiO2 by X-ray diffraction technique, S. Afr. J. Chem. Eng. 49 (2024) 348–352.
[67] M.A. Alam, R.K. Bishwas, S. Mostofa, S.A. Jahan, Crystallographic phase stability of nanocrystalline polymorphs TiO2 by tailoring hydrolysis pH, S. Afr. J. Chem. Eng. 49 (2024) 73–85.
[68] M.A. Alam, S.I. Sadia, M.K.H. Shishir, R.K. Bishwas, S. Ahmed, S.M. Al-Reza, et al., Crystallinity integration and crystal growth behavior study of preferred oriented (111) cubic silver nanocrystal, Inorg. Chem. Commun. 173 (2025) 113834.
[69] M. Adil, S. Alam, U. Amin, I. Ullah, M. Muhammad, M. Ullah, et al., Efficient green silver nanoparticles-antibiotic combinations against antibiotic-resistant bacteria, AMB Express 13 (2023) 115.
[70] H. Hassan Afandy, D.K. Sabir, S.B. Aziz, Antibacterial activity of the green synthesized plasmonic silver nanoparticles with crystalline structure against gram-positive and gram-negative bacteria, Nanomaterials 13 (2023) 1327.
[71] S. Narkhede, P. Parkhey, A. Dadsena, A. Singhai, E. Phillips, V. Kolla, et al., Green synthesis of silver nanoparticles for arsenic (III) removal from contaminated water, J. Chem. Health Risks 14 (2024) 1851–1868.
[72] N. Thirumagal, A.P. Jeyakumari, Structural, optical and antibacterial properties of green synthesized silver nanoparticles (AgNPs) using Justicia adhatoda L. leaf extract, J. Cluster Sci. 31 (2020) 487–497.
[73] D. Lahiri, M. Nag, H.I. Sheikh, T. Sarkar, H.A. Edinur, S. Pati, et al., Microbiologically-synthesized nanoparticles and their role in silencing the biofilm signaling cascade, Front. Microbiol. 12 (2021) 636588.
[74] H.F. Hetta, I.M.S. Al-Kadmy, S.S. Khazaal, S. Abbas, A. Suhail, M.A. El-Mokhtar, et al., Antibiofilm and antivirulence potential of silver nanoparticles against multidrug-resistant Acinetobacter baumannii, Sci. Rep. 11 (2021) 10751.
[75] N. Bhardwaj, S. Puri, A. Kumari, A. Chauhan, A. Kumar, Phyto-mediated synthesis of copper oxide nanoparticles: an investigation of antioxidant, antimicrobial, anti-inflammatory, and protective neuropsychiatric potential, BioNanoScience 14 (2024) 5377–5409.
[76] D. Mazumder, R. Mittal, S.K. Nath, Green synthesis of silver nanoparticles from waste Vigna mungo plant and evaluation of its antioxidant and antibacterial activity, Biomass Convers. Biorefinery 15 (2025) 5839–5850.
[77] A. Gurtu, M.S. Bakshi, Ag nanometallic surfaces for self-assembled ordered morphologies of zein, ACS Omega 3 (2018) 10851–10857.
[78] M. Hassanisaadi, G.H.S. Bonjar, A. Rahdar, S. Pandey, A. Hosseinipour, R. Abdolshahi, Environmentally safe biosynthesis of gold nanoparticles using plant water extracts, Nanomaterials 11 (2021) 2033.
[79] O. Pryshchepa, P. Pomastowski, B. Buszewski, Silver nanoparticles: synthesis, investigation techniques, and properties, Adv. Colloid Interface Sci. 284 (2020) 102246.
[80] H. Jensen, J.H. Pedersen, J. J∅ rgensen, J.S. Pedersen, K.D. Joensen, S.B. Iversen, et al., Determination of size distributions in nanosized powders by TEM, XRD, and SAXS, J. Exp. Nanosci. 1 (2006) 355–373.
[81] I. Gheorghe-Barbu, V.M. Corbu, C.O. Vrancianu, I.C. Marinas, M. Popa, Dumbravă Aş, et al., Phenotypic and genotypic characterization of recently isolated multidrug-resistant Acinetobacter baumannii clinical and aquatic strains and demonstration of silver nanoparticle potency, Microorganisms 11 (2023) 2439.
[82] K.D. Martínez-García, T. Zertuche-Arias, J. Bernáldez-Sarabia, E. Iñiguez, T. Kretzchmar, T.A. Camacho-Villegas, et al., Radical scavenging, hemocompatibility, and antibacterial activity against MDR Acinetobacter baumannii in alginate-based aerogels containing lipoic acid-capped silver nanoparticles, ACS Omega (2024).
[83] D.R. Monteiro, L.F. Gorup, A.S. Takamiya, E.R. de Camargo, A.C.R. Filho, D. B. Barbosa, Silver distribution and release from an antimicrobial denture base resin containing silver colloidal nanoparticles, J. Prosthodont.: Implant, Esthetic Reconstructive Dentistry 21 (2012) 7–15.
[84] R. Behdad, M. Pargol, A. Mirzaie, S.Z. Karizi, H. Noorbazargan, I. Akbarzadeh, Efflux pump inhibitory activity of biologically synthesized silver nanoparticles against multidrug-resistant Acinetobacter baumannii clinical isolates, J. Basic Microbiol. 60 (2020) 494–507.
[85] M. Fatemi, A. Meshkini, M.M. Matin, A dual catalytic functionalized hollow mesoporous silica-based nanocarrier coated with bacteria-derived exopolysaccharides for targeted delivery of irinotecan to colorectal cancer cells, Int. J. Biol. Macromol. (2024) 129179.
[86] D. Gupta, A. Singh, A.U. Khan, Nanoparticles as efflux pump and biofilm inhibitor to rejuvenate bactericidal effect of conventional antibiotics, Nanoscale Res. Lett. 12 (2017) 454.
[87] F.Y. Ahmed, U.F. Aly, R.M. Abd El-Baky, N.G. Waly, Effect of titanium dioxide nanoparticles on the expression of efflux pump and quorum-sensing genes in MDR Pseudomonas aeruginosa isolates, Antibiotics 10 (2021) 625.
[88] H. Barabadi, F. Mojab, H. Vahidi, B. Marashi, N. Talank, O. Hosseini, et al., Green synthesis, characterization, antibacterial and biofilm inhibitory activity of silver nanoparticles compared to commercial silver nanoparticles, Inorg. Chem. Commun. 129 (2021) 108647.
[89] Y.K. Mohanta, I. Chakrabartty, A.K. Mishra, H. Chopra, S. Mahanta, S.K. Avula, et al., Nanotechnology in combating biofilm: a smart and promising therapeutic strategy, Front. Microbiol. 13 (2023) 1028086.
[90] M. Anjugam, B. Vaseeharan, A. Iswarya, M. Divya, N.M. Prabhu, K. Sankaranarayanan, Biological synthesis of silver nanoparticles using β-1, 3 glucan binding protein and their antibacterial, antibiofilm and cytotoxic potential, Microb. Pathog. 115 (2018) 31–40.